

# Influence of indium segregation on the light emission of piezoelectric InGaAs/GaAs quantum wells grown by molecular beam epitaxy

C.M. Yee-Rendón, M. López-López, and M. Meléndez-Lira

*Departamento de Física, Centro de Investigación y de Estudios Avanzados del IPN,  
Apartado Postal 14-740, 07000 México, D. F., Mex.*

Recibido el 17 de septiembre de 2003; aceptado el 11 de noviembre de 2003

Pseudomorphic  $In_{0.2}Ga_{0.8}As/GaAs$  quantum wells (QWs) were grown by molecular beam epitaxy (MBE) on GaAs substrates oriented along the (11n) direction, with  $n=1,2,3,4$ . The optical and structural properties of the heterostructures were studied by photoluminescence spectroscopy (PL) at 14, 77 and 300 K, and atomic force microscopy (AFM) measurements. The emission wavelength from the QWs has two contributions, a blue shift due to the compressive strain, and a red shift due to the quantum confined Stark effect produced by the piezoelectric field present in these materials. A traditional theoretical interpretation of the QWs emission employing a simple well model shows discrepancies with the experimental results. In order to satisfactorily explain the emission wavelength we proposed to include segregation effects of In at the wells interfaces. The matrix transfer method was implemented to solve numerically the Schrödinger equation taking into account In segregation effects by including an asymmetric potential well with a profile depending on the details of the In incorporation. With segregation effects included in the emission calculations, the theoretical predictions reproduce very well the experimental values of PL emission. Our results demonstrate that in order to have efficient InGaAs QWs-based optoelectronic devices is very important to take into account interfacial segregation effects.

**Keywords:** Quantum wells; piezoelectric field; Indium segregation.

Se crecieron pozos cuánticos pseudomórficos de InGaAs/GaAs por epitaxia de haces moleculares sobre sustratos de GaAs orientados en la dirección (11n),  $n=1,2,3,4$ . Se estudiaron las propiedades ópticas y estructurales por medio de fotoluminiscencia (FL) a 14, 77 y 300 K, y microscopía de fuerza atómica (MFA). La emisión de los pozos cuánticos tiene dos contribuciones, un corrimiento hacia el color azul debido al esfuerzo compresivo al que está sujeto la heteroestructura y un corrimiento hacia el rojo debido al efecto Stark cuántico producido por el campo piezoeléctrico presente en estos materiales. Para explicar satisfactoriamente la energía de emisión de los pozos cuánticos proponemos incluir efectos de segregación de In en la interfaz de los pozos cuánticos. Implementamos el método de la matriz de transferencia para resolver numéricamente la ecuación de Schrödinger incluyendo los efectos de la segregación en el potencial de los pozos. Con la inclusión de los efectos de segregación en los cálculos de la emisión, las predicciones teóricas reproducen muy bien los resultados de FL.

**Descriptores:** Pozos cuánticos; campo piezoeléctrico; segregación de Indio.

PACS: 68.65.Fg; 78.67; 81.07.St

## 1. Introduction

Lately with the advent of novel growth techniques that have made possible to obtain high quality heteroepitaxial systems, the use of internal stress for material design is now a fact. The discovery of important electric fields in pseudomorphic structures [1], and so the potential to control the emission of these structures, has produced spectacular advances in the production of devices employing these materials. The InGaAs/GaAs system [2, 4] is the typical pseudomorphic heterostructure in which high piezoelectric fields, as high as the GaAs breakdown voltage, can be produced.

The objective of the present work focuses on the study of the structural and optical properties of InGaAs/GaAs quantum wells (QWs) with special emphasis on the growth orientation effects. Photoluminescence spectroscopy has been employed to obtain the emission energy of the transitions in the QWs. There are some differences between the experiments and the theoretical calculations employing a simple well model. The differences are greater for the samples that by atomic force microscopy presented a rougher surface, suggesting a strong influence of interfacial effects. In particular,

we addressed the problem of the disagreement between the piezoelectric field needed to fit the experimental QWs emission, and the theoretical piezoelectric field calculated from the strain. The discrepancy is more marked along the (111) direction, where 60-70% of the theoretical piezoelectric field is required to explain the experimental QWs emission [5, 6]. In order to explain this problem, some authors have proposed to include a charge density at the QWs interfaces that decrease the magnitude of the piezoelectric field [5], but with no clear explanation on the origin of this charge. Here, we propose to include In segregation effects [7, 14] at the InGaAs/GaAs interfaces as a solution to this discrepancy. The theoretical calculations of the QWs emission were carried out taking into account the effects associated with crystallographic orientations of the type (11n). With our proposal theoretical calculations and experimental measurements fit remarkably well.

## 2. Experimental Procedure

Samples with three  $In_xGa_{1-x}As/GaAs$  QWs of 100, 50, and 22 Å of nominal thickness were grown by molecular beam

epitaxy (MBE) . The nominal concentration of In was kept at 20% ( $x = 0.2$ ) for all the samples. The structures were grown over semi-insulating (111)-, (112)-, (113)-, and (114)-oriented GaAs substrates, as a reference a (001)-oriented sample was prepared. The native oxide layer was removed using  $H_2SO_4$ , and the wafers were rinsed in deionised water for 5 min before etching for 80 sec with  $NH_4OH:H_2O_2:H_2O$  (2:1:95) at  $25^\circ C$ . After etching, the wafers were rinsed in deionised water for 5 min and finally they were blown with nitrogen. All samples were immediately mounted on molybdenum holders without indium. The  $As_4$  beam equivalent pressure was  $2.2 \times 10^{-5}$  Torr and the  $As_4/Ga$  ratio was 6.5. After thermal cleaning at  $700^\circ C$  for one minute, a 200 nm GaAs buffer layer was grown at  $620^\circ C$ . The substrate temperature was decreased during the last few minutes of GaAs growth before starting the growth of InGaAs at  $560^\circ C$ . Figure 1 shows a sketch of the QWs structure in each sample which consists of a 50 nm  $Al_{0.35}Ga_{0.65}As$  barrier, followed by a 20 nm GaAs first barrier, then the first  $In_{0.20}Ga_{0.80}As$  well of 100Å, and a 20 nm GaAs second barrier. The same barrier structures were grown for the 50- and 25 Å QWs. After the growth atomic force microscopy (AFM) images from the surface of the samples were obtained in air conditions. Photoluminescence (PL) spectra at three different temperatures of 14, 77 and 300 K, were measured employing a standard equipment with the 632.8 nm line of a He-Ne laser.

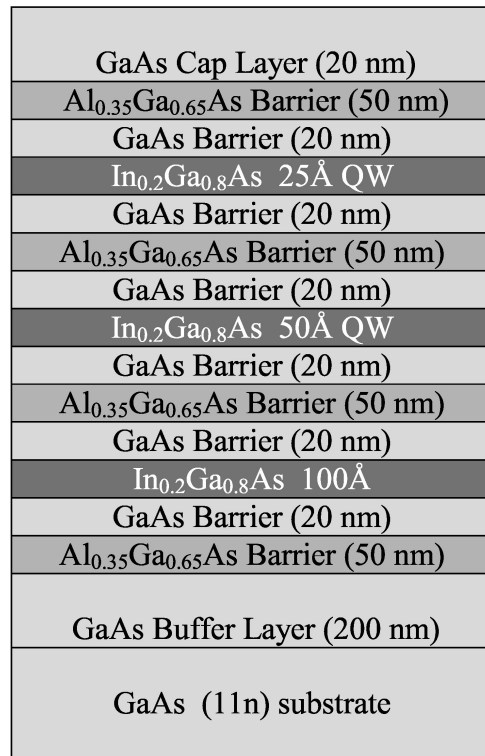


FIGURE 1. Scheme of the typical structure of the InGaAs quantum wells studied in this work.

### 3. Theory

The bulk lattice constant of the InGaAs alloy with 20% of In content is  $a_{InGaAs} = 0.5734$  nm, compared with that of GaAs ( $a_{GaAs} = 0.5653$  nm) there is a lattice mismatch given by  $\Delta a = a_{GaAs} - a_{InGaAs}$ . In a pseudomorphic growth, this lattice mismatch produces a biaxial compressive stress ( $e = \Delta a/a_{InGaAs} = 0.014$ ) in the InGaAs well layers. This stress produces shifts in the InGaAs band gap energy value, and it affects the conduction and valence bands alignment in the heterostructure [15,16]. In this work, in order to ob-

tain the potential profile at the conduction and valence bands we employed the following procedure. First we aligned the InGaAs/GaAs interface with no stress employing the solid model by Van der Walle [17, 18]. Then, the stress effects were included by the model of Pollak [15, 16]. A picture of the calculation process is presented in Fig. 2(a). So far, in this scheme we have considered only the band alignment between the GaAs barriers and the stressed InGaAs well layer. In order to obtain the complete potential acting on the carriers, we must include a piezoelectric field given by [19]:

$$P_i = e_{14}\epsilon_{kj} \quad k \neq j \quad (1)$$

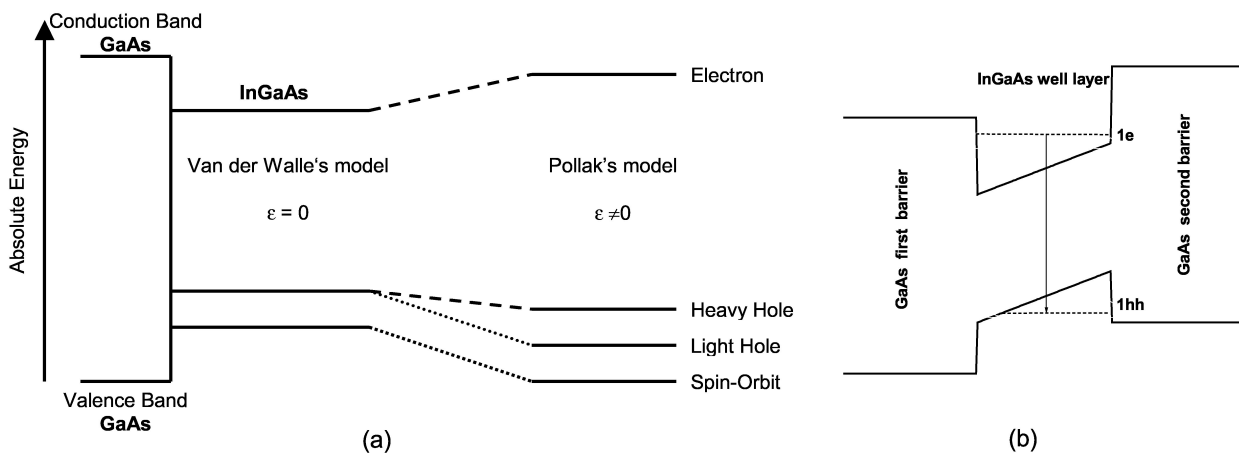


FIGURE 2. (a) Picture of the theoretical procedure employed to calculate the heterostructure potential profile. For (11n) oriented samples a piezoelectric field should be included. A sketch of the complete potential acting on the carriers is shown in Fig. 2(b). A more realistic potential should also include In segregation effects.

Where  $P_i$  is the induced polarization,  $e_{14}$  is the piezoelectric constant, and  $\epsilon_{kj}$  are the components of the deformation matrix produced by the biaxial stress. The piezoelectric field generated by the strain induced polarization is significant for (11n) directions, where there are non-hydrostatic components of the stress, and could be as high as 257 kV/m along the (111) direction. A sketch of the potential profile including the piezoelectric field is shown in Fig. 2(b). Finally, the complete potential profile was introduced into the Schrödinger equation to obtain the energy of the quantized levels in the wells. The matrix transfer method was implemented to numerically solve the Schrödinger equation within the effective mass formalism [20].

#### 4. Structural characterization

Figure 3 shows atomic force microscopy (AFM) images from the surface of the samples grown on: a) (001)- b) (114)-, c) (113)-, d) (112)- and e) (111)-oriented GaAs substrates. We observe a smooth surface morphology for the (001) orientation. An analysis of the root mean square (RMS) surface roughness values from AFM measurements is shown in Fig. 4. In this figure  $\theta$  is the polar angle between the (11n) substrate orientation and the [001] direction. We observe that most of the samples present flat surfaces with RMS values lower than 0.5 nm. The RMS values increases to 0.7 nm for the (111) orientation, the (112) sample presents the highest RMS value of 4.5 nm. The high RMS value for the (112)-oriented substrate reflects the difficulty to growth high quality samples in this direction. A high RMS value of sur-

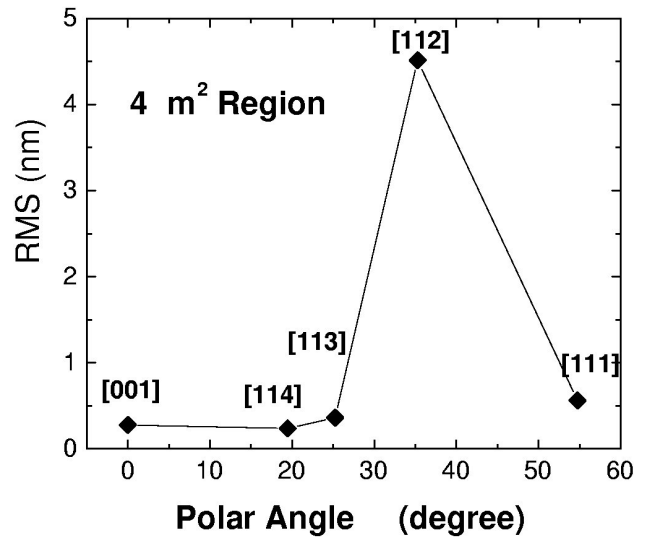


FIGURE 4. RMS surface roughness values obtained from the AFM analysis over a  $4\mu\text{m}^2$  region. Here  $\Theta$  is the angle between the [11n] substrate orientation and the [001] direction.

face roughness is commonly associated to a poor crystal quality, and as we will show below this is correlated with a wide and weak PL peak signal.

#### 5. Photoluminescence

Figure 5 shows photoluminescence (PL) spectra of the samples at three different temperatures of: a) 14, b) 77, and c) 300 K. In Fig. 5(a) the transition around 1.37 eV associated to the first electron level, to the first heavy hole level

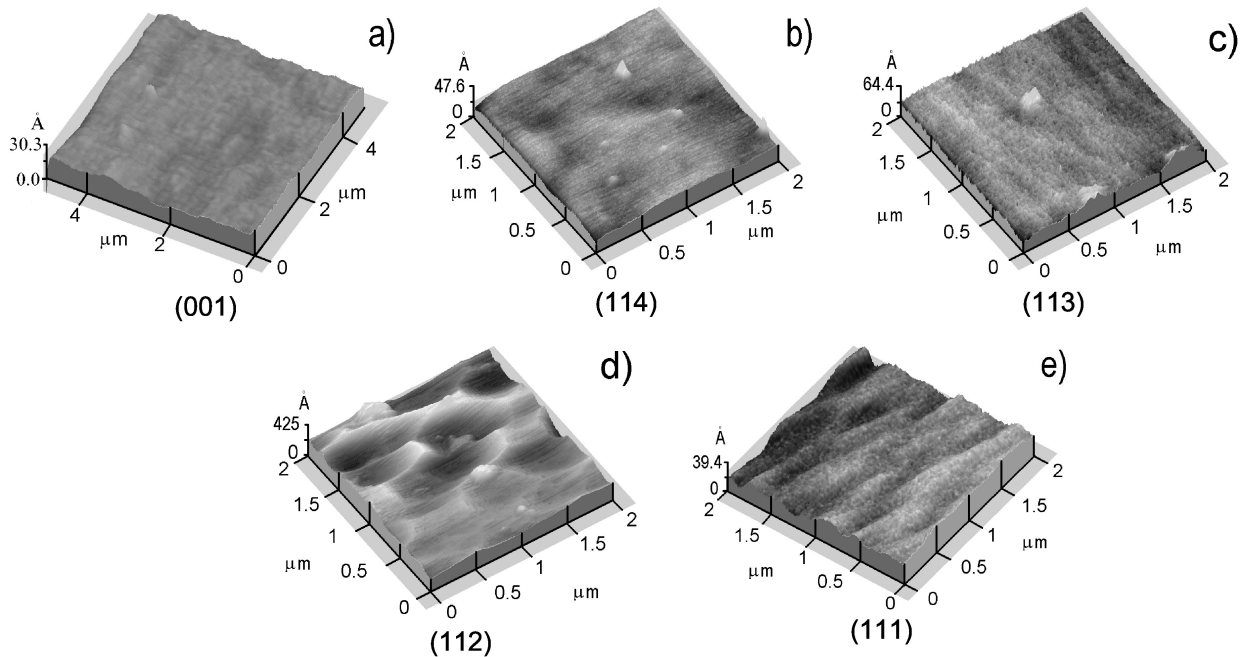


FIGURE 3. Atomic force microscopy images of samples surface oriented along a) (001)-, b) (114)-, c) (113)-, d) (112)- and e) (111) substrates.

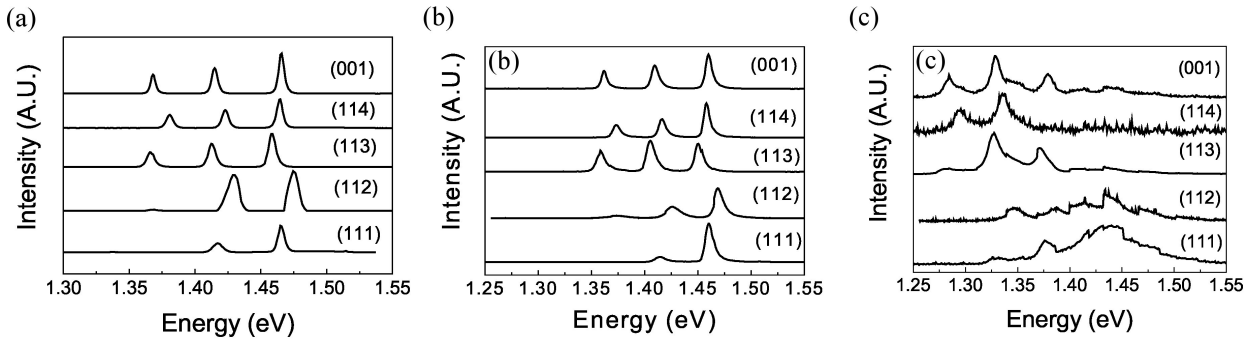


FIGURE 5. PL spectra from the QWs grown on the different substrates taken at three different temperatures: a) 14 , b) 77 and c) 300 K.

(1e-1hh) in the 10 nm QW appears extremely weak for the (112)- and (111)-oriented samples. We think that this could be caused by a partial strain relaxation which produces non-radiative recombination centers in these QW's. An analysis of the full width at half maxima (FWHM) of PL spectra at 14 K is shown in Fig. 6. Narrow PL peaks of less than 6.5 meV in FWHM are present for all the QWs in the (001)-, (113)-, and (114)-samples, which confirms a high crystalline quality of these samples. The FWHM of PL peaks are wider for the (112) and (111) directions, in particular for the thicker QWs, reflecting rough interfaces. These results are in agreement with AFM observations. It should be noted that the emission energy from InGaAs/GaAs QWs has two main contributions, a shift to blue colour product of the band gap increment by the compressive stress in InGaAs [15], and a red shift due to the Quantum Confinement Stark Effect (QCSE) [1]. Both contributions depend on the orientation of the substrate. The experimental values of the PL peak energies were fitted to the results of a theoretical calculation of the 1e-1hh transitions in simple InGaAs QWs with ideal interfaces, like that illustrated in Fig. 2(b). However, in order to reasonably fit the observed PL peaks energy it was necessary to reduce the piezoelectric fields magnitude, and to use non nominal In concentrations. In table 1 we summarize the percentage of the theoretical

TABLE I. Percentage of the In nominal concentration (%In), and percentage of the theoretical piezoelectric field intensity (%Pi) necessary to fit the 1e-1hh QWs transition energy in the PL spectra. For the calculation we employed a simple QW model as shown in Fig. 2(b).

Sample orientacion	%In	%Pi
(001)	18	---
(114)	18.5	85
(113)	19.9	70
(112)	19.8	55
(111)	20.25	64

piezoelectric field intensity, and the percentage of the nominal In concentration that we employed to fit the 1e-1hh QWs energy transition for each substrate orientation. We observe that we need to significantly change the piezoelectric field magnitude and the In concentration to explain the PL peaks energy. This problem has also been found by other authors [5,6].

In order to solve the above explained problem we propose to include segregation effects in the heterostructures with the following model:

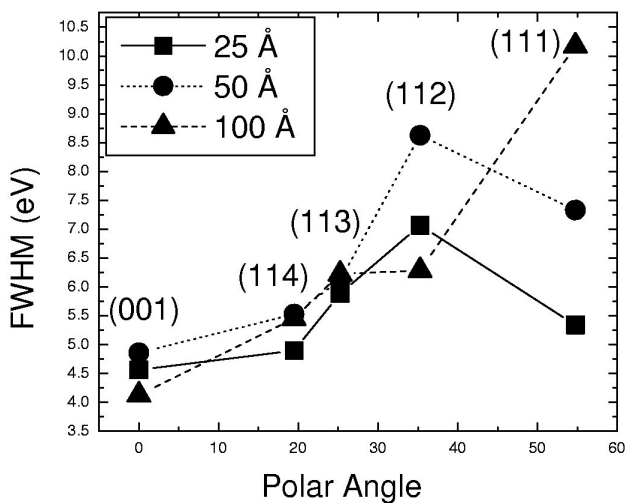


FIGURE 6. Analysis of the FWHM from PL peaks at 14K associated to the principal QWs emissions.

$$x_n = x_0(1 - \sigma_1^n) \quad 1 \leq n \leq N, \quad \text{inside the well} \quad (2)$$

$$x_n = x_0(1 - \sigma_1^N)\sigma_2^{n-N} \quad n \leq N, \quad \text{in the second GaAs barrier} \quad (3)$$

Here  $x_n$  is the In concentration at the n-esime monolayer,  $x_0$  is the nominal In concentration, and N is the nominal width in number of monolayers.  $\sigma_i$  is given by:

$$\sigma_i = e^{-\frac{d(11n)}{\lambda_j}} \quad (4)$$

Where d (11n) is the interplanar length along the (11n) direction, and  $\lambda_i$  is the In segregation length at the first (i=1)

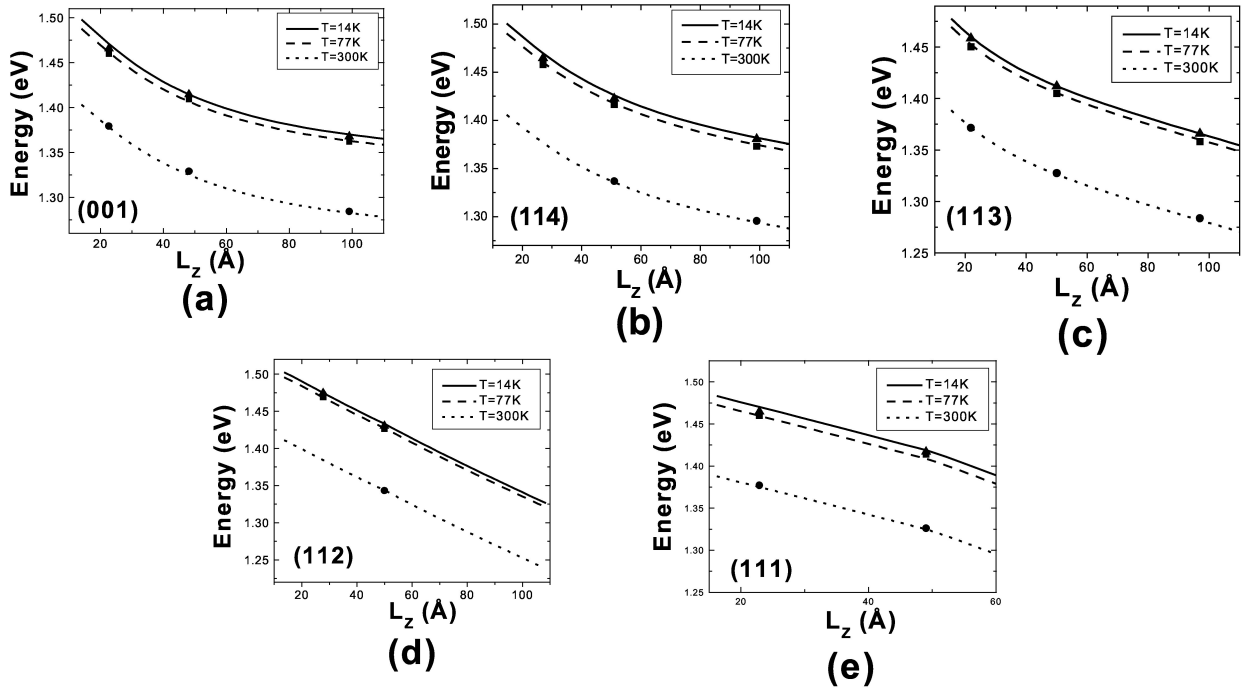


FIGURE 7. Plots of the 1e-1hh transition energies calculated with In segregation vs. QWs thickness for: a) (001)-, b) (114)-, c) (113)-, d) (112)-, and e) (111) substrate orientation. The continuous, dashed and dotted lines represent our results calculated at 14, 77, and 300 K, respectively. The PL peaks energy obtained from the measurements at three different temperatures are plotted by: (▲)14 K, (■)77 K, and (●)300 K.

and second ( $i=2$ ) interface in each QW. It is convenient to remark that both,  $d(11n)$  and  $\lambda_i$  depend on the substrate orientation. Moreover  $\lambda_i$  has a more complicated dependence on growth conditions such as the substrate temperature and In flux. The segregation of In will produce changes in the effective QWs electric potential, making that the wells shape differs from the simple model illustrated in Fig. 2(b). We obtained the 1e-1hh transition energy solving the Schrödinger equation by the method described in section 3, but now including the changes in the QWs by the In segregation, and with segregation lengths as free fit parameters. Figure 7 shows graphs of the calculated 1e-1hh transition energy as a function of QW thickness for: a) (001)-, b) (114)-, c) (113)-, d) (112), and e) (111) substrate orientation. In this figure the continuous, dashed and dotted lines represent our results calculated at 14, 77, and 300 K, respectively. For comparison in Fig. 7 we also plotted the PL peaks energy obtained in the PL measurements at the three different temperatures of (▲)14K, (■)77K, and (●)300K. We observe that employing the In segregation model our theoretical calculations of the 1e-1hh transitions fit remarkably well the observed PL QW emissions at the three different temperatures. It is important to note that the theoretical piezoelectric field magnitudes were used in our calculations, and nominal In concentrations were employed as initial QW parameters. The segregation lengths obtained from PL fits are reported in table 2, and are in agreement with common accepted values for InGaAs/GaAs heterostructures [8]. The different values for segregation lengths are the result of different growth conditions and substrate

TABLE II. Segregation lengths  $\lambda_1$  and  $\lambda_2$  obtained from the fit of the PL spectra employing the In segregation model.

Sample orientation	well width (Å)	$\lambda_1$ (Å)	$\lambda_2$ (Å)
(001)	25	5	2
	50	5	2
	100	5	2
(114)	25	7	5
	50	7	3
	100	7	3
(113)	25	6	6
	50	6	6
	100	6	6
(112)	25	20	10
	50	20	4
	100	20	4
(111)	25	27	12
	50	27	4
	100	27	4

orientation, even if all the samples were grown at the same time, the thermodynamic processes in each direction are not equal. It is interesting to note that we obtained two different segregation lengths for a specific substrate orientation. The first segregation length  $\lambda_1$  is associated to the growth of InGaAs over the first GaAs barrier, this process is determined by the incorporation of In into the GaAs matrix to produce the InGaAs alloy, and so once that growth conditions are fixed it

should be the same for any well width on a given orientation. The second segregation length  $2$  is produced during the growth of the second GaAs barrier over the InGaAs layer. The incorporation of In into the GaAs upper barrier depends on the total amount of In segregated at the InGaAs surface in the growth process of each QW, and thus it depends on the well width. From table 2 we observe that surface segregation lengths associated to the growth of InGaAs, that is  $\lambda_1$ , depend on the crystal orientation in the following order:

$$\lambda_{(001)} < \lambda_{(113)} < \lambda_{(114)} < \lambda_{(112)} < \lambda_{(111)} \quad (5)$$

This order is in accordance to reported values obtained from different methods [8]. In Fig. 8 we present plots of the In concentration profiles as a function of QW thickness ( $L_z$ ) for: a) (001)-, b) (114)-, c) (113)-, d) (112), and e) (111) orientated substrates. In this figure we can observe how a different  $\lambda_1$  strongly affects the In concentration profile shape. We observe that the In concentration increases exponentially from  $x=0$ , at the first QW interface, and asymptotically reaches the nominal concentration ( $x=0.20$ ) at a thickness determined by the particular value of  $\lambda_1$ . The difference between the nominal In concentration and the calculated In concentration at a given thickness ( $L_z$ ), is the amount of In non incorporated at this growth stage, which is segregated onto the InGaAs growing surface.

Now, the amount of In segregated at the InGaAs surface should be incorporated into the second GaAs barrier, this process is determined by  $\lambda_2$ . As we can see in Fig. 8, the amount of In segregated on the InGaAs surface is greater for QWs with small  $L_z$ , therefore in order to consume all the segregated In atoms a longer ( $L_z$ ) is required for thinner wells.

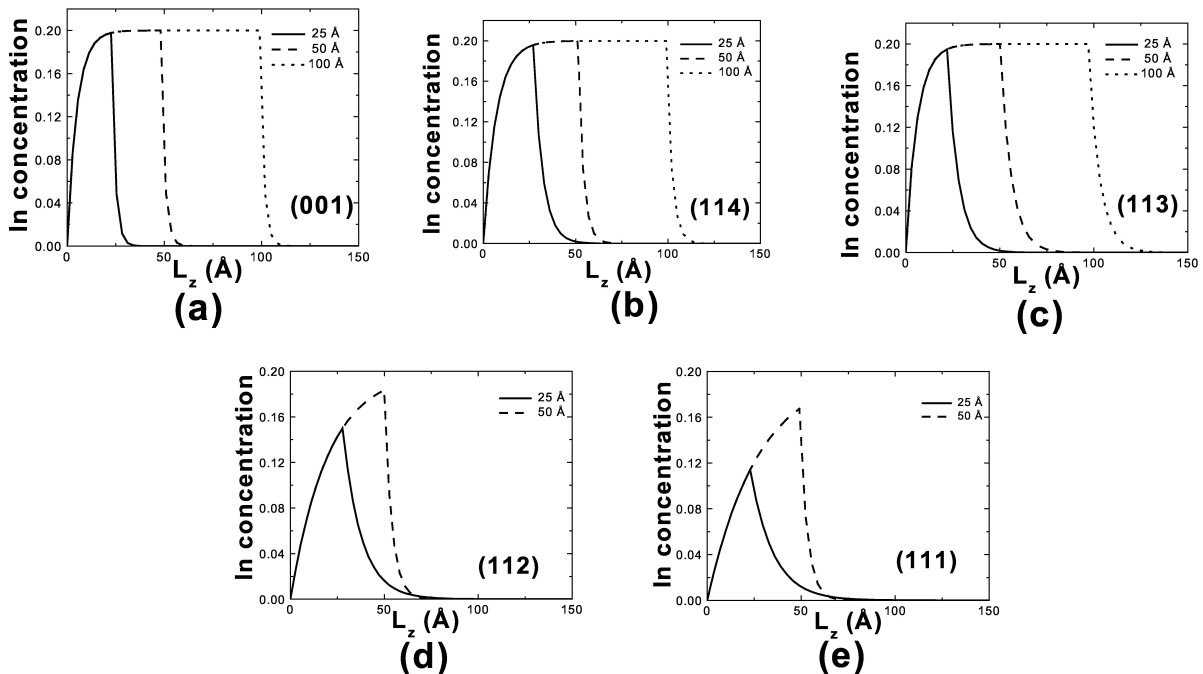


FIGURE 8. In concentration profiles for QWs grown on: a) (001)-, b) (114)-, c) (113)-, d) (112)- and e) (111) substrates. The continuous, dashed and dotted lines represent the profiles for QWs of 25, 50 and 100 Å in width.

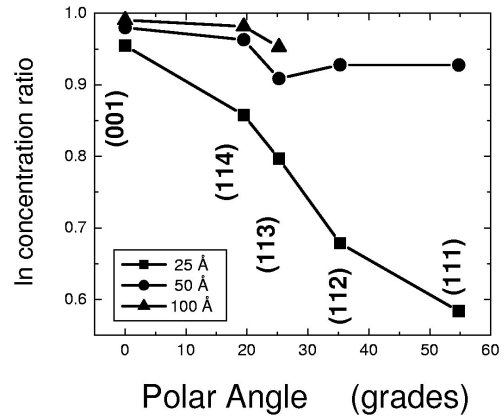


FIGURE 9. Ratio of the amount of In inside the well layer to the total amount of In in the structure (well layer and upper barrier), for QWs of width of (■)25Å, (●)50Å, and(▲)100Å.

Finally, in Fig. 9 we report the ratio of the amount of In incorporated in the InGaAs well layer to the total amount of In incorporated in the structure including the GaAs upper barrier, for QW thickness of: (▲)100Å, (●)50Å, and (■)25Å. We observe that for the (001) orientation almost all the In atoms reside inside the well layer, this explains why a simple well potential model of Fig. 2(b) accurately predicts the PL emission energy for QWs grown on (001) substrates. From Fig. 9 we note that in general the simple well model is also a good approximation for QWs grown on (114)- and (113) GaAs substrates [21, 23], except for thinner wells. In contrast for the (112)- and (111) orientation, where In segregation plays a major role, the simple well model fails to explain the PL spectra.

## 6. Conclusion

We have proposed an In segregation model at the QWs interfaces to explain the electronic transitions in InGaAs/GaAs QWs. We found that by including In segregation effects is possible to accurately predict the PL peaks energy associated to the 1e-1hh transitions. With the In segregation model is not necessary to arbitrarily reduce the piezoelectric fields magnitude to explain the PL peaks energy. An important result is that In segregation should be taken into account in the study of this kind of structures. Finally, we found that the QWs grown on (113) substrates presented superior properties

since they have sharp PL emission peaks, smaller segregation lengths, and have a high piezoelectric field intensity. These characteristics could be useful to develop optoelectronic devices that take advantage of the intrinsic piezoelectric fields present in InGaAs/GaAs QWs.

## Acknowledgments

The authors would like to thank the technical support of Erasmo Gomez and Rogelio Fragoso. This work was partial supported by CONACyT.

- 
1. D.A.B. Miller, Phys. Rev. Lett. **53**, (1984) 2173.
  2. Zhores I Alferov, Rev. Mod. Phys. **73**, (2001) 767.
  3. Herbert Kromer, Rev. Mod. Phys. **73**, (2001) 783.
  4. G. C. Osbourn, Phys. Rev. B. **27**, (1983) R5308.
  5. Pablo O. Vaccaro, Mitsuo Takahashi, Kazuhisa Fujita and Toshihide Watanabe, J. Appl. Phys. **76**, (1994) 8037.
  6. R.A. Hogg et al, Phys. Rev. B. **48**, (1993) 8491.
  7. Haiping Yu, Christine Roberts and Ray Murray, Appl. Phys. Lett. **66**, (1995) 2253.
  8. Matthias Ilg and Klaus H. Ploog, Phys. Rev. B. **48**, (1993) 11512.
  9. K. Muraki, S. Fakatsu, Y. Shiraki and R. Ito, J. Cryt Growth **127**, (1993) 546.
  10. Koichi Ymaguchi, Tesuya Okada and Fumito Hiwatashi, Appl. Surf. Sci. **117**, (1997) 700.
  11. Hiroshi Yamaguchi and Yoshiji Horikoshi, J. Appl. Phys. **85**, (1999) 2221.
  12. Philippe Ballet et al, Phys. Rev. B. **59**, (1999) R5308.
  13. Jiang, S.C. Shen, S.M. Wang and T.G. Andersson, Appl. Phys. Lett. **66**, (1995) 1948.
  14. Sam Dong Kim et al, J. Vac. Sci. Technol. B. **14**, (1996) 642.
  15. Fred H. Pollak, "Effect of homogeneous strain on the electronic and vibrational levels on semiconductors", Chapter 2. Strained-Layer Superlattices, edited by Thomas P. Pearshall, Academic Press.
  16. Fred. H. Pollak, Surf. Sci. **37**, (1973) 863.
  17. Cris G. Van de Walle, Mat. Res. Soc. Symp. Proc. **12** (1988).
  18. Cris G. Van de Walle, Phys. Rev. B **39**, (1989) 1871.
  19. Richard M. Martin, Phys. Rev. B **5**, (1972) 1607.
  20. Björn Jonsson and Sverre T. Eng, IEEE J. Quatum Electronics **26**, (1990) 2025.
  21. S.H. Pan et al, Phys. Rev. B **38**, (1988) 3375.
  22. S.F. Yoom, K. Radhakrishan and H.M. Li, Superlatt. and Mic. **14**, (1993) 79.
  23. Pablo O. Vaccaro, Mitsuo Takahashi, Kazuhisa Fujita and Toshihide Watanabe, Jap. J. Appl. Phys. **34**, (1995) 13.